Antiferromagnetism and the gap of a Mott insulator: Results from analytic continuation of the self-energy

Xin Wang,[1] Emanuel Gull,[1,2] Luca de' Medici,[3] Massimo Capone,[4] and Andrew J. Millis[1]
[1]*Department of Physics, Columbia University, New York, New York 10027, USA*
[2]*ETH Zürich, 8093 Zürich, Switzerland*
[3]*Laboratoire de Physique des Solides, Université Paris-Sud, CNRS UMR 8502, F-91405 Orsay Cedex, France*
[4]*SMC Center, CNR-INFM and Dipartimento di Fisica, Università di Roma "La Sapienza," Piazzale A. Moro 2, I-00185 Rome, Italy and ISC-CNR, Via dei Taurini 18, I-00185 Rome, Italy*
(Received 13 April 2009; revised manuscript received 15 June 2009; published 2 July 2009)

Direct analytic continuation of the self-energy is used to determine the effect of antiferromagnetic ordering on the spectral function and optical conductivity of a Mott insulator. Comparison of several methods shows that the most robust estimation of the gap value is obtained by use of the real part of the continued self-energy in the quasiparticle equation within the single-site dynamical mean-field theory of the two-dimensional square lattice Hubbard model, where, for a U that is slightly greater than the Mott critical value, antiferromagnetism increases the gap by about 80%.

DOI: 10.1103/PhysRevB.80.045101 PACS number(s): 71.10.Fd, 71.27.+a, 71.30.+h

I. INTRODUCTION

Quantum Monte Carlo (QMC) evaluations of imaginary-time path integrals[1–4] have improved to the point where they constitute one of the basic techniques of condensed-matter physics. Even for fermionic problem, where the sign problem precludes direct simulation, the theoretical developments associated with single-site[5] and cluster[6,7] dynamical mean-field theories (DMFTs) have enabled a powerful approximate solution in terms of a quantum impurity model, which for not too large clusters is sign-free or at least has a tractable sign problem. However, while the QMC methods have proven to be very powerful in the study of static expectation values, obtaining dynamical information has remained challenging. The available techniques are based either on an exact diagonalization (ED) method,[8,9] where the number of states that contribute to a given response function is so small that level spacings become an issue, or on the analytic continuation of imaginary-time data,[10–12] which involves a host of other uncertainties.

The difficulties appear with particular force in the context of the question of whether the high-T_c cuprates are Mott insulating materials.[13] Recent work has suggested that the value of the gap and the form of the conductivity in the above-gap region provide important insights into the physics of Mott and charge-transfer insulators.[14–16] A question of particular interest is the change in gap value associated with onset of antiferromagnetic (AFM) order in a Mott insulator. One recent paper argued in favor of negligible changes[16] while another argued for a large change.[14] However, determining with precision the gap value in theoretical model of correlated material is not straightforward. Figure 1 illustrates some of the uncertainties. It shows three estimations of the local spectral function (many-body density of states) for a theoretical model (described more fully below) of a Mott insulator: one obtained by an ED method and two obtained by maximum entropy (MaxEnt) (Ref. 12) analytic continuation of imaginary-time QMC data. While the qualitative structure of the three estimations appears consistent, there are significant differences in detail, including a factor of two in the size of the gap that makes it difficult to compare the theoretical results to data.

In this paper we present a critical examination of different methods of determining the spectral function of a Mott insulator, and apply the results to the question of the gap value, spectral function, and optical conductivity in the paramagnetic (PM) and antiferromagnetic phases of the two-dimensional square lattice Hubbard model. We study MaxEnt analytic continuation of the Green's function and of the self-energy, and compare the results to ED calculations and to direct thermodynamic evaluations of the gap. We argue that continuation of the self-energy provides the best method

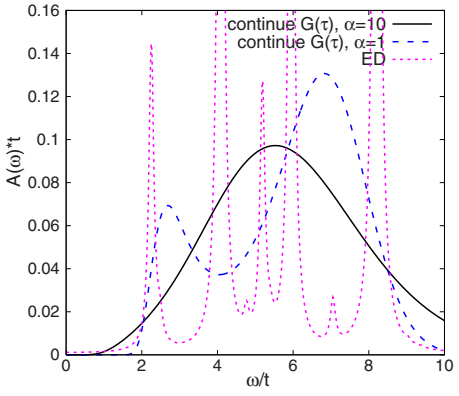

FIG. 1. (Color online) Paramagnetic phase spectral function of the two-dimensional square lattice half-filled Hubbard model with nearest-neighbor hopping and interaction parameter $U=12t$ computed using single-site DMFT with an ED impurity solver (dotted lines) or an imaginary-time hybridization expansion continuous-time QMC impurity solver followed by an analytic continuation of the measured Green's function (solid and dashed lines). Due to particle-hole symmetry $A(\omega)=A(-\omega)$ only positive frequency is shown. QMC is done at inverse temperature $\beta t=10$; α is a parameter in analytic continuation procedure, which will be explained below.

 ©2009 The American Physical Society

of minimizing the broadening effect of MaxEnt procedure. The self-energy is also needed for computation of other response functions, for example, the optical conductivity. We establish that for U near the Mott critical value the onset of antiferromagnetism increases the gap of the half-filled square lattice Hubbard model by about $3.4t$ relative to that of the paramagnetic case, thus increasing the gap by about 80%.

The rest of this paper is organized as follows. In Sec. II we define the model to be studied and the methods of solution, discuss MaxEnt, and in particular its application to the self-energy. Section III presents a detailed analysis of the results from analytic continuation and also summarizes the interpretation of exact diagonalization data in light of these results. Section IV discusses the optical conductivity, and Sec. V is a summary and conclusion.

II. FORMALISM

A. Model

We study the two-dimensional Hubbard model defined by the Hamiltonian

$$H = \sum_{p,\sigma} \varepsilon_p c^\dagger_{p,\sigma} c_{p,\sigma} + U \sum_i \left(n_{i,\uparrow} - \frac{1}{2} \right) \left(n_{i,\downarrow} - \frac{1}{2} \right), \tag{1}$$

with $\varepsilon_p = -2t(\cos p_x + \cos p_y) - \mu$. We choose the chemical potential $\mu = 0$ such that the electron density $n = 1$. We are interested in the imaginary part of the real-axis electron Green's function.

To solve the model we employ the single-site dynamical mean-field approximation,[5] which makes the approximation that the self-energy is a function of frequency only $\Sigma(p,\omega) \to \Sigma(\omega)$. On this assumption Eq. (1) may be mapped on to a quantum impurity model with parameters determined by a self-consistency condition. The essential computational task is to solve the quantum impurity model to obtain the local Green's function $G_{\rm loc}$ and self-energy $\Sigma(\omega)$. We have used two methods: a recently developed hybridization expansion continuous-time QMC procedure[3] and an ED method.[8,9] The ED method approximates physical response functions as a series of poles. The QMC methods produce estimates of Green's functions and self-energies in imaginary time. One must then analytically continue the QMC results to obtain physically relevant real frequency quantities. To perform the analytic continuation we used the MaxEnt methods pioneered in the condensed-matter physics context by Gubernatis and co-workers.[10–12]

The qualitative behavior of the model is well understood. For $n = 1$ and any $U > 0$, the ground state is antiferromagnetically ordered, and the single-particle spectrum is characterized by a gap, $\Delta(U)$, which we would like to compute. For $U > U_{c2} \approx 12t$ there is a gap in the spectrum even if antiferromagnetism is suppressed, and we are also interested in the value of this gap, and in the behavior of the spectral functions for frequencies near the gap edge.

To analyze the situation more precisely we note that in an insulator we expect $\mathrm{Im}\, G(\omega + i0^+) = 0$ for $|\omega| < \Delta$. We may write the Green's function (in general a matrix) as

$$\mathbf{G}(p,\omega) = [\omega \mathbf{1} - \mathbf{H}_0(p) - \Sigma(p,\omega)]^{-1}. \tag{2}$$

$\mathrm{Im}\, \mathbf{G}(p,\omega) \neq 0$ either when $\mathrm{Im}\, \mathbf{\Sigma}(p,\omega) \neq 0$ or, regardless of the value of $\mathrm{Im}\, \mathbf{\Sigma}$, if the "quasiparticle equation"

$$\det[\omega \mathbf{1} - \mathbf{H}_0(p) - \mathrm{Re}\, \mathbf{\Sigma}(p,\omega)] = 0 \tag{3}$$

is satisfied for some momentum p.

In the single-site DMFT the PM phase quasiparticle equation is

$$\omega - \mathrm{Re}\, \Sigma(\omega) = -2t(\cos p_x + \cos p_y). \tag{4}$$

In the AFM phase we have

$$\mathbf{G}^{-1} = \begin{pmatrix} \omega - \Sigma_\uparrow(\omega) & 2t(\cos p_x + \cos p_y) \\ 2t(\cos p_x + \cos p_y) & \omega - \Sigma_\downarrow(\omega) \end{pmatrix}, \tag{5}$$

and the quasiparticle equation is

$$[\omega - \mathrm{Re}\, \Sigma_\uparrow(\omega)][\omega - \mathrm{Re}\, \Sigma_\downarrow(\omega)] = 4t^2(\cos p_x + \cos p_y)^2. \tag{6}$$

We may therefore define two gaps: $\Delta_{\mathrm{Im}\,\Sigma}$, the lowest frequency at which $\mathrm{Im}\, \Sigma \neq 0$, and $\Delta_{\rm qp}$, the lowest frequency at which the quasiparticle equation is satisfied. If the interaction is nonvanishing, for $\omega > \Delta_{\rm qp}$ phase space is available for a particle to decay so that we expect $\Delta_{\rm qp} \geq \Delta_{\mathrm{Im}\,\Sigma}$. Empirically we found $\Delta_{\rm qp} \lesssim \Delta_{\mathrm{Im}\,\Sigma}$, suggesting that $\Delta_{\rm qp} \simeq \Delta_{\mathrm{Im}\,\Sigma}$ for the Hubbard model.

We may also define a third gap Δ_μ from the dependence of the particle density n on chemical potential μ. This is given in terms of the momentum-integrated spectral function $A_\sigma = -\mathrm{Im}\, G_\sigma / \pi$ for spin σ by

$$n(\mu) = \sum_\sigma \int d\omega f(\omega - \mu) A_\sigma(\omega, \mu), \tag{7}$$

where $f(\omega) = 1/[\exp(\beta\omega) + 1]$ is the Fermi function. If the spectral function changes smoothly with μ then for μ that is only slightly larger than Δ, we would have, at $T = 0$,

$$n(\mu) = 1 + 2 \int_\Delta^\mu d\omega A(\omega, \mu = 0) + \mathcal{O}(\mu - \Delta)^2, \tag{8}$$

so that $n(\mu)$ would change from one when $\mu = \Delta$. However, it is known[17–19] that, in the PM Mott insulating region of the single-site DMFT, the spectral function changes nontrivially with chemical potential, introducing "in-gap" states so that n begins to differ from unity at $\mu = \Delta_{\rm PM} - A_0 t$ with A_0 as a number of order unity. It is not known whether this phenomenon occurs in the AFM phase. The μ at which n begins to deviate from unity therefore provides a lower bound on the gap in the insulating state.

B. Analytic continuation

In practice QMC generates a numerical estimate $\bar{F}$ of a function $F(\tau)[F(i\omega_n)]$ defined on imaginary time (or Matsubara frequency). For fermionic correlators F is related to a spectral function $A(\omega)$ by

$$F(\tau) = \int_{-\infty}^{\infty} d\omega \frac{e^{-\tau\omega}}{1+e^{-\beta\omega}} A(\omega), \tag{9}$$

with $\beta = 1/T$ as the inverse temperature.

Analytic continuation is the inversion of Eq. (9) to determine A given F. Unfortunately, the matrix defined by $\exp(-\tau\omega)/[\exp(-\beta\omega)+1]$ is extremely poorly conditioned, with many relatively small eigenvalues that, on inversion, greatly amplify any errors in $\bar{F}$ (i.e., differences between QMC estimate $\bar{F}$ and true value F), leading to highly unreliable estimates of A. While various attempts have been made to avoid this problem, the most widely used one is the MaxEnt method.[10–12] MaxEnt is based on defining A as the function that extremizes a cost functional $Q[\{A\}]$, which is the sum of entropylike (S) and energylike (L) terms:

$$Q[\{A\}] = \alpha S[\{A\}] - L[\{A\}]. \tag{10}$$

In Eq. (10), α is a temperaturelike quantity that controls the competition between S and L. The energylike term is defined in terms of the mean-square misfit between the proposed spectrum computed from Eq. (9) and the QMC data $\bar{F}$, which in the matrix form is

$$L = \frac{1}{2}(\bar{\mathbf{F}} - \mathbf{KA})^T \mathbf{C}^{-1} (\bar{\mathbf{F}} - \mathbf{KA}). \tag{11}$$

Here $\mathbf{C}$ is a correlation matrix that represents the uncertainties (statistical and systematic) in the computation:

$$C_{ij} = \langle \delta F(\tau_i) \delta F(\tau_j) \rangle. \tag{12}$$

The crucial part of the method is the entropylike term, which is defined in terms of a model function $m(\omega)$ as

$$S = \int d\omega \left[A(\omega) - m(\omega) - A(\omega) \ln \frac{A(\omega)}{m(\omega)} \right]. \tag{13}$$

The model function is chosen to encapsulate prior information about the function A: in the problems of physical relevance this typically includes positivity and a known normalization. We use a Gaussian model function $1/(\sqrt{2\pi}\sigma)\exp[-x^2/(2\sigma^2)]$ with $\sigma = 5t$ and we have checked that the results do not depend on the width of this Gaussian. To perform the minimization we use the algorithm of Ref. 12. We generate spectra using a broad range of α and select the spectrum corresponding to the most probable α, according to Ref. 12, by calculating the posterior probability of α at a given $\bar{G}$, $P(\alpha|\bar{G})$, which, up to a normalization factor, is:

$$P(\alpha|\bar{G}) = \prod_i \left(\frac{\alpha}{\alpha + \lambda_i} \right)^{1/2} \frac{e^{Q(\hat{A})}}{\alpha}, \tag{14}$$

where $\hat{A}$ is the resulting spectrum and λ_i are the eigenvalues of $\{A^{1/2}\}\nabla\nabla L|_{\hat{A}}\{A^{1/2}\}$. Here $\{A^{1/2}\}$ means a matrix with elements $\sqrt{A_i}\delta_{ij}$.

Note that uncertainties of error bar estimation from binning of Monte Carlo data and neglect of off-diagonal correlation matrix elements (explained below) may introduce errors in selected α from $P(\alpha|G)$. In the following context we shall show that a reliable determination of gap size does not change with reasonable variance of α.

C. Self-energy

The feature of our work is the direct continuation of the self-energy that is related to the full Green's function G and the noninteracting Green's function G_0 by

$$\Sigma = G_0^{-1} - G^{-1}. \tag{15}$$

In the Hubbard model, the self-energy has the following asymptotic behavior:[20]

$$\Sigma_\sigma(i\omega_n) = U\langle n_{-\sigma}\rangle + U^2\langle n_{-\sigma}\rangle(1-\langle n_{-\sigma}\rangle)\frac{1}{i\omega_n} + O\left(\frac{1}{(i\omega_n)^2}\right). \tag{16}$$

If the Hartree term $U\langle n_{-\sigma}\rangle$ is subtracted, the remaining is just like the Green's function with a different normalization $U^2\langle n_{-\sigma}\rangle(1-\langle n_{-\sigma}\rangle)$. We also introduce the cutoff frequency ω^* to avoid the error in high frequencies and replace the self-energy with frequencies above ω^* by its known asymptotic behavior (16). Thus frequencies above ω^* will not be included in the MaxEnt procedure and their value should be correctly reproduced if we satisfy the normalization condition. We have also verified that including points at $\omega > \omega^*$ does not change our result since (as discussed below) the $\mathrm{Im}\,\Sigma$ at higher Matsubara frequencies have a much larger error estimation thus contributing much smaller weight in calculating L.

It is important to properly treat the noise correlations and encode them in the correlation matrix. In our work we do not consider errors in G_0. Thus if G has an average value of $\bar{G}$ and a measurement error of δG then by expanding

$$\delta\Sigma(i\omega_n) = \bar{G}^{-2}(i\omega_n)\delta G(i\omega_n) + \bar{G}^{-3}(i\omega_n)\delta G(i\omega_n)^2 + \cdots. \tag{17}$$

Therefore Σ has a possibly nonzero shift:

$$\langle \delta\Sigma(i\omega_n)\rangle = \bar{G}^{-3}(i\omega_n)\langle \delta G(i\omega_n)^2\rangle + \cdots, \tag{18}$$

and a correlator

$$\langle \delta\Sigma(i\omega_n)\delta\Sigma^*(i\omega_m)\rangle = \bar{G}^{-2}(i\omega_n)\bar{G}^{*-2}(i\omega_m)\langle \delta G(i\omega_n)\delta G^*(i\omega_m)\rangle + \cdots. \tag{19}$$

Structure in G means that there are important correlations in Σ; in particular, because at large ω, $G \sim 1/\omega$, the high-frequency fluctuations in Σ are large.

We estimate $G(\tau)$ from continuous-time measurements binned into uniformly discretized bins of width $\Delta\tau$. Suppose that in imaginary time the fluctuations in G are δ correlated and independent of time (this may always be ensured by an appropriate measurement process)

$$\langle \delta G(\tau_i)\delta G(\tau_j)\rangle = g^2\delta_{ij}. \tag{20}$$

Then (assuming τ are evenly discretized on $[0,\beta)$ with size $\Delta\tau$)

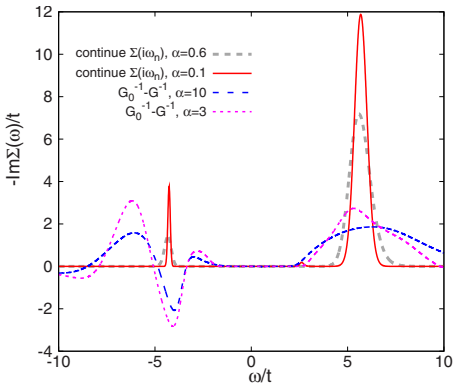

FIG. 2. (Color online) Comparison of minority spin Im $\Sigma(\omega)$ computed by subtracting continued G_0^{-1} and G^{-1} (long- and short-dashed lines), and continuing Σ (thick dashed and the solid lines) for $\beta t=10$, $U=12t$ is the half-filled square lattice in the antiferromagnetic phase. We see that the $G_0^{-1}-G^{-1}$ one does not preserve positive definiteness.

$$\langle \delta G(i\omega_n)\delta G^*(i\omega_m)\rangle = \beta g^2(\Delta\tau)\delta_{\omega_n,\omega_m}. \tag{21}$$

Note that $g^2\Delta\tau$ is expected to be independent of bin size $\Delta\tau$. Then Eq. (18) gives zero and Eq. (19) gives

$$\langle \delta\Sigma(i\omega_n)\delta\Sigma^*(i\omega_m)\rangle = \bar{G}^{-2}(i\omega_n)\bar{G}^{*-2}(i\omega_m)\beta g^2(\Delta\tau)\delta_{\omega_n,\omega_m}, \tag{22}$$

which is the correlation matrix we need. Observe that this means that in this case the orthogonal transformation that diagonalizes the covariance matrix is the transformation to Matsubara frequencies.

D. Continuing $G(\tau)$

The self-energy may alternatively be computed by first continuing G_0 and G, inverting the continued functions, and subtracting. Figure 2 compares the imaginary part of self-energy computed in this way to the result obtained by continuing $\Sigma(i\omega_n)$. We present two α values for each computation: one chosen to be near the peak of $P(\alpha|\bar{G})$ ($\alpha=3$) and one at a somewhat larger α ($\alpha=10$).

The quantity $G_0^{-1}-G^{-1}$ is not guaranteed to be positive definite and we see that an unphysical sign indeed occurs. The difficulties are that G and G_0 are small at high frequency so that errors in the MaxEnt procedure are amplified on inversion. Errors in the position of the gap edge are also amplified in Σ. Finally, the calculated structures in Σ are too broad. Another deficiency is seen in the PM insulating phase (not shown here) where $G_0^{-1}-G^{-1}$ fails to correctly represent the pole at the chemical potential, which is known to exist in Σ.

III. RESULTS

A. Method

The DMFT calculation was performed with the hybridization expansion continuous-time QMC solver.[3] Typically more than 10^9 Monte Carlo steps are made in each DMFT iteration, which usually takes around 1 h CPU time on a cluster with 40 2 GHz processors. Special attention must be paid in the paramagnetic insulating phase: in order to resolve the pole in $\Sigma(\omega)$ one needs a real frequency grid that has very high resolution in the vicinity of the chemical potential.

We use α values that range several orders of magnitude to do analytic continuation. For each given α we calculate $P(\alpha|\bar{G})$ at the convergence, use Kramers-Kronig relation to get Re $\Sigma(\omega)$ from computed Im $\Sigma(\omega)$, and do a momentum integral of Eq. (2) to get the Green's function.

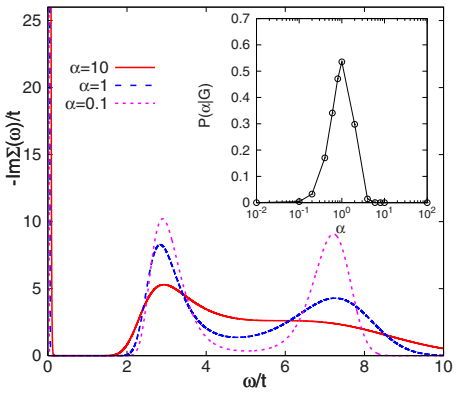

FIG. 3. (Color online) Main panel: Imaginary part of PM self-energy for $\beta t=10$, $U=12t$, and $\mu=0$ with several α's. Inset: the posterior probability $P(\alpha|\bar{G})$ as a function of α. Note the log scale of α. At $\alpha=10$ [above the maximum of $P(\alpha|\bar{G})$] the result is very smooth. At $\alpha=1$ [at the maximum of $P(\alpha|\bar{G})$] more detailed features appear, which become more pronounced for $\alpha=0.1$ [below the maximum of $P(\alpha|\bar{G})$].

B. PM phase

The main panel of Fig. 3 shows the imaginary part of continued self-energies calculated with three α value for the paramagnetic insulating phase of the two-dimensional square lattice Hubbard model. We see a clear pole near the chemical potential but the detailed structures in side bands $2t<\omega<8t$ vary. The inset shows $P(\alpha|\bar{G})$ with a maximum at $\alpha=1$. For $\alpha=10$ [above the maximum of $P(\alpha|\bar{G})$], Im Σ is smooth because of the regularization from model function. For $\alpha=1$ [at the maximum of $P(\alpha|\bar{G})$], more structure is observed. For $\alpha=0.1$ [below the maximum of $P(\alpha|\bar{G})$] these detailed features are more pronounced. The differences in the curves give some idea of the uncertainties in the process. The maximum in posterior probability identifies the $\alpha=1$ curve as the preferred continuation.

The left panel of Fig. 4 shows the real part of continued self-energies. The α values are the same as those in Fig. 3. The pole at $\omega=0$ in Im Σ implies Re $\Sigma\sim 1/\omega$ at low frequencies. The crossing point between Re Σ and $\omega+4t$ curves gives the minimal positive solution to the quasiparticle equation, which gives an estimated half-gap size around $\omega=2.1t$. Turning to the right panel, which is the spectral function plotted at the same ω scale, we see that the estimate size of $2.1t$ is consistent with all four curves: ED puts its first peak

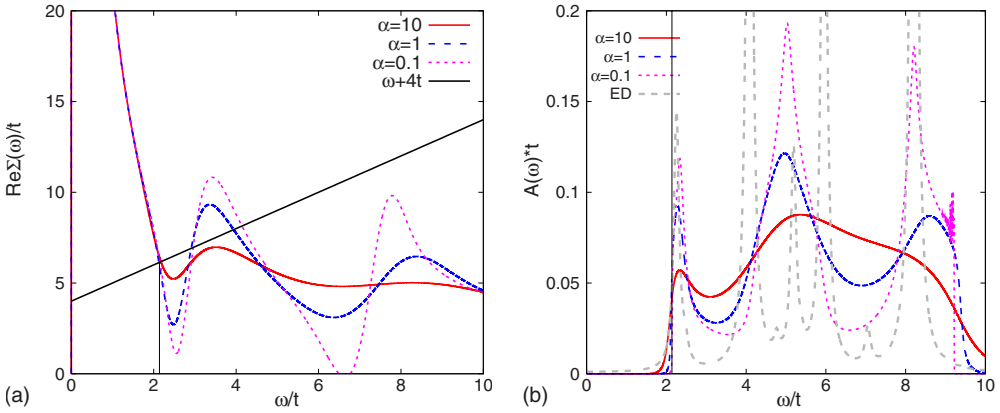

FIG. 4. (Color online) Left panel: real part of PM self-energies for $\beta t=10$, $U=12t$, and $\mu=0$ for several values of α, along with quasiparticle equation Re $\Sigma(\omega)=\omega+4t$. The quasiparticle equation has a minimum positive solution at around $\omega=2.1t$. Right panel: spectral function constructed from the continued self-energy along with the result from ED. Vertical lines at $\omega=2.1t$ are drawn as eye guide. We see that all curves are consistent with the estimated half-gap size $\omega=2.1t$.

slightly above $\omega=2.1t$, and the nonzero structure of QMC curves below $\omega=2.1t$ could be safely considered as a result of broadening in MaxEnt procedure. The interesting fact is that the estimate of gap size is robust against a reasonable variation in α, which provides an indication that the gap estimate is reliable.

Figure 5 shows the averaged total electron density as a function of chemical potential at $U=12t$ and various different temperatures. This does not need analytic continuation, thus providing an independent check of the MaxEnt results. If we assume $A(\omega)$ changes slowly with temperature, then thermal fluctuation gives $\langle n(T)\rangle=\langle n(T=0)\rangle+AT^2$ with A as a positive number if μ is close to the lower edge of the upper Hubbard band. However, on the contrary, $\langle n\rangle$ increases as temperature is decreased in Fig. 5. This suggests the existence of in-gap states that increase rapidly as temperature is reduced. Moreover, for the lowest available temperature $\beta t=20$ curve, we see an almost linear dependence close to the band edge ($2t<\omega<2.5t$), which is also a result of in-gap states. Extrapolation of the $\langle n(\mu)\rangle$ curve gives $\Delta_\mu=1.8t$ that, considering the presence of in-gap states, is consistent with the discussion in Sec. II that $\Delta_{qp}-\Delta_\mu=0.3t$.

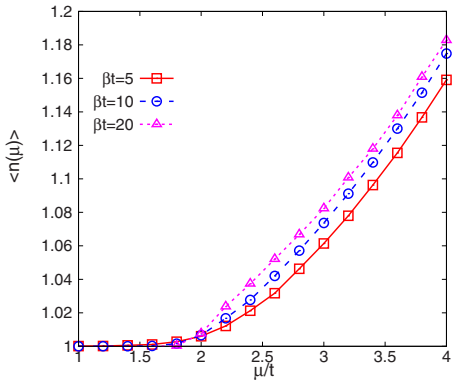

FIG. 5. (Color online) Averaged total electron density as a function of chemical potential $\langle n(\mu)\rangle$ for paramagnetic $U=12t$ square lattice at inverse temperatures $\beta t=5,10,20$. We see that $\Delta_\mu=1.8t$.

C. AFM phase

The main panel of Fig. 6 is the continued imaginary part of $\Sigma(\omega)$. The inset shows the corresponding $P(\alpha|\bar{G})$ curve. We see that the $\alpha=0.1$ curve is sharper than the curves for $\alpha=0.6,1$. This is very similar with what we found in PM case.

The left panel of Fig. 7 shows the minimum positive solution to the quasiparticle equation. We get a half-gap size around $3.8t$. This is also robust against changing α with a variance as small as $0.1t$. The dash-dotted line shows the Hartree-Fock (HF) mean-field solution. The averaged magnetization produced by Hartree-Fock $\langle m\rangle=0.94$ agrees with the QMC value but it predicts a half-gap size of $5.6t$ that is much larger than the QMC value.

The right panel of Fig. 7 shows the minority-spin AFM spectral function constructed from the continued self-energy $[A_{\text{majority}}(\omega)=A_{\text{minority}}(-\omega)]$. The behavior at the gap edge is very sharp. The sharpness comes from the combined effect

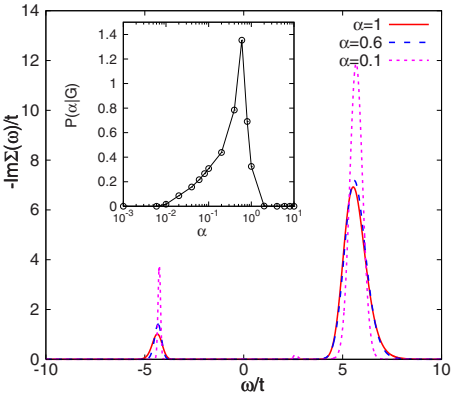

FIG. 6. (Color online) Main panel: imaginary part of AFM minority-spin self-energy for $\beta t=10$, $U=12t$, and $\mu=0$ with several values of α. Inset: $P(\alpha|\bar{G})$ versus α curve. We again see that the continued self-energy has sharper features at $\alpha=0.1$ [below the maximum of $P(\alpha|\bar{G})$] than at $\alpha=0.6,1$ [at or above the maximum of $P(\alpha|\bar{G})$].

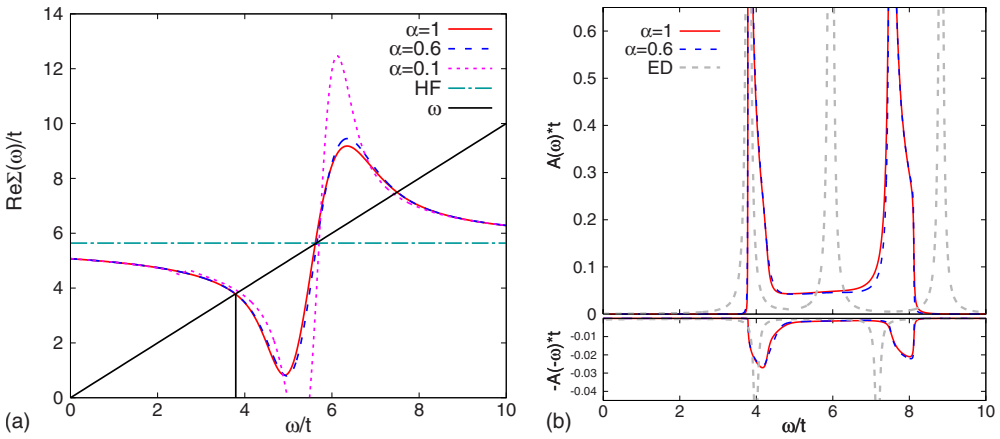

FIG. 7. (Color online) Left panel: real part of AFM self-energy for $\beta t=10$, $U=12t$, and $\mu=0$ with several values of α, and the quasiparticle equation $\mathrm{Re}\,\Sigma(\omega)=\omega$. The HF mean-field prediction is also shown. The quasiparticle equation has a solution at $\omega=3.8t$. A vertical line is drawn at $\omega=3.8t$ as an eye guide. Right panel: spectral function constructed from the continued self-energy along with ED result. Due to the particle-hole symmetry $A_{\mathrm{majority}}(\omega)=A_{\mathrm{minority}}(-\omega)$, only minority spin is shown. The removal peak of spectral function has been reflected to positive frequency and shown in the bottom of the right panel. The estimate of gap edge $\omega=3.8t$ is consistent with the reconstructed spectral function.

of Fermi-surface nesting and mass renormalization. The half-gap size is consistent with $\Delta_{\mathrm{qp}}=3.8t$. As in the PM phase, ED also put its first peak at the gap edge. At higher frequency there is a clear difference between ED and QMC calculations: QMC has one additional peak at around $7.5t$ while ED has two peaks at $6t$ and $9t$, and in particular, the estimate of the upper band edge is different. As noted in Sec. I, ED and QMC+MaxEnt make different approximations, and thus produces different self-energies (especially at high frequencies), which translates to a difference in estimate of upper band edge mathematically. However, at current stage we do not have definite statements about its physical origin.

Figure 8 shows the averaged total electron density as a function of μ when AFM order is allowed. As in PM phase, this provides an independent check of MaxEnt results. For the temperature studied ($\beta t=10$), $\Delta_\mu \simeq 3.6t \lesssim \Delta_{\mathrm{qp}}$. This is again consistent with the discussion in Sec. II. We also see that the gap will get larger when temperature is reduced. Within our precision we cannot distinguish whether in-gap

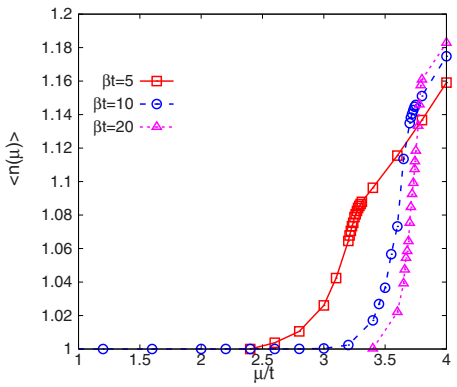

FIG. 8. (Color online) Averaged total electron density as a function of chemical potential $\langle n(\mu)\rangle$ for the Hubbard model on a square lattice using a self-consistency condition that allows for AFM order, at $U/t=12$, and inverse temperature $\beta t=5$, 10, and 20.

states exist in this case. We see that varying the chemical potential in the insulating phase leads at low T to a very sharp transition [visible as a slope discontinuity in the $n(\mu)$ curves] between a paramagnetic metal phase and an antiferromagnetic insulating phase. Even at our lowest temperature $\beta t=20$ the $\langle n(\mu)\rangle$ curve is apparently continuous and is associated with a rapid (but also apparently continuous) change in staggered magnetization (not shown here). Whether the transition becomes first order as $T\to 0$ remains to be studied. On increasing μ from zero the transition occurs at $\Delta_\mu \lesssim \Delta_{\mathrm{qp}}$. (At $\beta t=10$, $\Delta_\mu \simeq 3.6t$ and $\Delta_{\mathrm{qp}}=3.8t$.)

IV. OPTICAL CONDUCTIVITY

The optical conductivity can be computed using the Kubo formula and the minimal-coupling ansatz $\mathbf{p}\to\mathbf{p}-\mathbf{A}$. The dissipative part of the conductivity is then[21]

$$\sigma(\Omega)=\frac{2e^2}{\hbar}\int_{-\infty}^{\infty}\frac{d\omega}{\pi}\int\frac{d^2p}{(2\pi)^2}\frac{f(\omega)-f(\omega+\Omega)}{\Omega}$$

$$\times\mathrm{Tr}[\mathbf{j}(p)\mathrm{Im}\,\mathbf{G}(\omega+\Omega,p)\mathbf{j}(p)\mathrm{Im}\,\mathbf{G}(\omega,p)], \quad (23)$$

where the current operator is $\mathbf{j}=\delta\mathbf{H}/\delta p_x$.

Figure 9 compares the paramagnetic and antiferromagnetic phase optical conductivities. We see that PM optical conductivity has a gap $\simeq 4.2t$ and a relatively soft edge while in AFM phase it has a gap of $\simeq 7.6t$ and a sharp edge. This is a consequence of the large change in gap due to antiferromagnetism. The high-T_c cuprates are believed to be described by $t\approx 0.38$ eV (this value is, for example, the average of the even- and odd-parity values quoted in the table in Sec. VII of Ref. 22). Our result would imply that if U in the cuprates were of the order of U_{c2} the optical gap would be about 2.9 eV, rather larger than the observed $2\Delta\approx 1.8$ eV.

V. CONCLUSION

To conclude, we have presented a method to find the gap size from QMC DMFT calculations. We first continue the

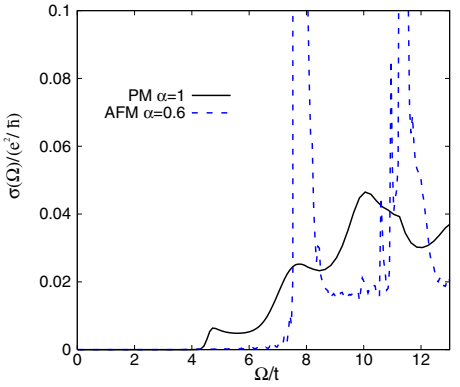

FIG. 9. (Color online) Optical conductivities constructed from analytically continued QMC data for half-filled Hubbard model on a square lattice at $U=12t$ and inverse temperature $\beta t=10$. The PM curve has a gap at $\Omega \simeq 4.2t$ and the AFM curve has a sharp gap edge at $\Omega \simeq 7.6t$.

measured $\Sigma(i\omega_n)$ to $\Sigma(\omega)$, using MaxEnt with the correctly estimated correlation matrix, and select α from the peak in the posterior probability $P(\alpha|\bar{G})$. We then plot Re $\Sigma(\omega)$ and find the lowest positive solutions to the quasiparticle equation. Curves corresponding to different values of α may give slightly different estimates but this variation has been found to be small. We find that within our numerical accuracy the gap edge is defined by the quasiparticle equation [Eq. (3)] so (at least within the single-site DMFT) there are no in-gap excited states arising from, e.g., an excitonic binding between a particle and a spin wave. In the paramagnetic phase doping produces in-gap states; we have established that the shift is about $0.3t$ at $U \gtrsim U_{c2}$.

For the $U=12t \gtrsim U_{c2}$ Hubbard model on the square lattice, we found a half-gap size of $2.1t$ in the PM phase and $3.8t$ in the AFM phase. Thus for $U \gtrsim U_{c2}$ antiferromagnetic order increases the gap relative to that of the paramagnetic solution by about 80%. This has been qualitatively noted in Refs. 14 and 23, which applied QMC and ED, respectively, to a model with a semicircular density of states, but our method provides a reliable quantitative result for the square lattice model. Our finding supports the conclusions of Ref. 14 that U must be somewhat less than the Mott critical value in the cuprates. The difference of gap size is also apparent in the calculated optical conductivity, in particular the AFM optical conductivity is remarkably sharp near the gap edge, and has a corresponding sharp feature at the upper edge of the upper Hubbard band. We believe this is special to the square lattice, arising from the perfect nesting.

ACKNOWLEDGMENTS

We thank D. Reichman for helpful discussions. X.W. and A.J.M. are supported by NSF Contract No. DMR-0705847, E.G. by NSF Contract No. DMR-0705847 and the Swiss National Science Foundation, L.d.M. by RTRA Triangle de la physique, and M.C. by MIUR Contract No. PRIN2007 2007FW3MJX. Some of the calculations have been done using the ALPS library (Ref. 24).

[1] R. Blankenbecler, D. J. Scalapino, and R. L. Sugar, Phys. Rev. D **24**, 2278 (1981).
[2] J. E. Hirsch and R. M. Fye, Phys. Rev. Lett. **56**, 2521 (1986).
[3] P. Werner, A. Comanac, L. de' Medici, M. Troyer, and A. J. Millis, Phys. Rev. Lett. **97**, 076405 (2006).
[4] P. Werner and A. J. Millis, Phys. Rev. B **74**, 155107 (2006).
[5] A. Georges, G. Kotliar, W. Krauth, and M. J. Rozenberg, Rev. Mod. Phys. **68**, 13 (1996).
[6] T. Maier, M. Jarrell, T. Pruschke, and M. Hettler, Rev. Mod. Phys. **77**, 1027 (2005).
[7] G. Kotliar, S. Y. Savrasov, K. Haule, V. S. Oudovenko, O. Parcollet, and C. A. Marianetti, Rev. Mod. Phys. **78**, 865 (2006).
[8] M. Caffarel and W. Krauth, Phys. Rev. Lett. **72**, 1545 (1994).
[9] M. Capone, L. de' Medici, and A. Georges, Phys. Rev. B **76**, 245116 (2007).
[10] R. N. Silver, D. S. Sivia, and J. E. Gubernatis, Phys. Rev. B **41**, 2380 (1990).
[11] J. E. Gubernatis, M. Jarrell, R. N. Silver, and D. S. Sivia, Phys. Rev. B **44**, 6011 (1991).
[12] M. Jarrell and J. E. Gubernatis, Phys. Rep. **269**, 133 (1996).
[13] M. Imada, A. Fujimori, and Y. Tokura, Rev. Mod. Phys. **70**, 1039 (1998).
[14] A. Comanac, L. de' Medici, M. Capone, and A. J. Millis, Nat. Phys. **4**, 287 (2008).
[15] L. de' Medici, X. Wang, M. Capone, and A. Millis, arXiv:0804.2250 (unpublished).
[16] C. Weber, K. Haule, and G. Kotliar, Phys. Rev. B **78**, 134519 (2008).
[17] D. S. Fisher, G. Kotliar, and G. Moeller, Phys. Rev. B **52**, 17112 (1995).
[18] H. Kajueter, G. Kotliar, and G. Moeller, Phys. Rev. B **53**, 16214 (1996).
[19] P. Werner and A. J. Millis, Phys. Rev. B **75**, 085108 (2007).
[20] M. Potthoff, T. Wegner, and W. Nolting, Phys. Rev. B **55**, 16132 (1997).
[21] A. J. Millis, A. Zimmers, R. P. S. M. Lobo, N. Bontemps, and C. C. Homes, Phys. Rev. B **72**, 224517 (2005).
[22] O. K. Andersen, A. I. Liechtenstein, O. Jepsen, and F. Paulsen, J. Phys. Chem. Solids **56**, 1573 (1995).
[23] G. Sangiovanni, A. Toschi, E. Koch, K. Held, M. Capone, C. Castellani, O. Gunnarsson, S.-K. Mo, J. W. Allen, H.-D. Kim, A. Sekiyama, A. Yamasaki, S. Suga, and P. Metcalf, Phys. Rev. B **73**, 205121 (2006).
[24] A. F. Albuquerque, F. Alet, P. Corboz, P. Dayal, A. Feiguin, S. Fuchs, L. Gamper, E. Gull, S. Gürtler, A. Honecker, R. Igarashi, M. Körner, A. Kozhevnikov, A. Läuchli, S. R. Manmana, M. Matsumoto, I. P. McCulloch, F. Michel, R. M. Noackk, G. Pawłowski, L. Pollet, T. Pruschke, U. Schollwöck, S. Todo, S. Trebst, M. Troyer, P. Werner, S. Wessel, and the ALPS collaboration, J. Magn. Magn. Mater. **310**, 1187 (2007) doi:10.1016/j.jmmm.2006.10.304; http://alps.comp-phys.org/.